J Mater Sci: Mater Electron (2014) 25:573–580
DOI 10.1007/s10854-013-1625-0

A simple one-step solvothermal synthesis of hierarchically structured ZnO hollow spheres for enhanced selective ethanol sensing properties

Ying Zhang · Huiming Ji · Yalu Chen · Xiaohong Sun

Received: 27 August 2013 / Accepted: 15 November 2013 / Published online: 23 November 2013

Abstract A simple one-step solvothermal method, using ethanolamine as solvent without any additives except zinc source, has been employed to synthesize hierarchically structured ZnO hollow spheres consisting of numerous orderly and radical nanorods with diameter of several tens nanometers and length of 2–3 μm. The ethanolamine and the solvothermal process play the critical role in the synthesis of the ZnO hollow spheres by the primary formation of ZnO crystal nucleus and subsequent transformation into nanorods, which self-assemble into hollow spheres. The morphology and structure of the spheres have been characterized by transmission electron microscopy, field emission scanning electron microscopy, X-ray powder diffraction, high-resolution transmission electron microscopy, and Brunauer–Emmett–Teller N_2 adsorption–desorption analyses. The results also indicate that the sensor based on the prepared ZnO hollow spheres exhibit good ethanol sensing performance, which can be attributed to its structural defects and high surface-to-volume ratio that significantly facilitate the absorption of oxygen species and diffusion of target gas. Besides, the sensor shows high selectivity to ethanol because ZnO as a basic oxide is favored for dehydrogenation of ethanol.

1 Introduction

Zinc oxide (ZnO), an n-type semiconductor oxide with direct band gap (3.37 eV) and large exciton binding energy (60 meV) [1], has tremendous application in solar cells [2], gas sensors [3], photocatalysts and optoelectric transducers [4, 5], due to its special optical and electrical properties. It is well known that properties of ZnO are strongly related with its physical properties such as morphology, crystal structure, particle size, specific surface area and so on. Therefore, the designed ZnO nanomaterials with different morphologies and structures can significantly influence various properties. To date, various ZnO nanostructures have been fabricated, such as quantum dots [6], nanowires [7], nanorods [8], nanobelts [9], nanosheets [10], hollow spheres [11] and hierarchical structures [12].

In particular, hierarchical structures using lower dimension nanocrystals as the building blocks have attracted more interest because of their less gas diffusion length, higher mobility and relatively larger specific surface area than agglomerated nanoparticles, which lead to better gas sensing properties [13–16]. Many researchers have been devoted to constructing hierarchical ZnO architectures. Li et al. [17] have synthesized grid-structured ZnO microsphere arrays assembled by uniform ZnO nanorods by noncatalytic chemical vapor deposition. Wang et al. [18] prepared ZnO porous-shell hollow spheres by thermally oxidizing high-purity zinc powder in an oxygen-containing atmosphere. Jing and Zhan [19] obtained porous flower-like ZnO by annealing the plate-like ZnO precursor, which was prepared in the microwave system. Lea et al. [20] fabricated hierarchical porous ZnO microspheres by a facile hydrothermal method with subsequent calcinations. Zhang et al. [21] fabricated ZnO hierarchical architecture composed of flower-like plates by a one-pot solution method. Zhang et al. [22] developed a novel solvothermal process using ethylene glycol (EG) as solvent had been employed to synthesize 3D ZnO hollow micro-hemispheres consisting of numerous orderly and radical nanorods. From these reports, we know

Y. Zhang · H. Ji (✉) · Y. Chen · X. Sun
Key Laboratory for Advanced Ceramics and Machining Technology, Ministry of Education, School of Materials Science and Engineering, Tianjin University, Tianjin 300072, People's Republic of China
e-mail: jihuiming@tju.edu.cn

that hydrothermal/solvothermal reaction provides more facile chemical route to prepare highly crystalline ZnO or precursors, compared with chemical vapor deposition and thermal oxidation method. Under certain reaction conditions, the crystalline nano-building blocks such as nanoparticles, nanorods, nanoplates can be assembled into higher dimensional hierarchical structures. However, many hydrothermal/solvothermal reactions need many additives or could only obtain precursors. Thus, a simple, facile, and effective method to fabricate hierarchical ZnO architectures would be of great importance.

Herein, we present a novel and easy approach to synthesize hierarchically structured ZnO hollow spheres by self-assembly nanorods. This is simply done by solvothermal reaction of zinc acetate in the presence of ethanolamine. The sensor based on prepared products, which exhibits better gas sensing property compared with ZnO nanorods and high selectivity to ethanol. The sensing performance of the as-prepared ZnO materials working at a certain temperature heavily depends on their special structure as well as their surface-to-volume ratio. Moreover, the formation mechanisms for self-assembly of ZnO hollow spheres from nanorods have been primarily discussed.

2 Experimental

2.1 Synthesis and characterization of materials

All the chemicals used in the experiments were of analytical grade and used without further purification. In a typical procedure, 0.7024 g of $Zn(CH_3COO)_2{\cdot}2H_2O$ was dissolved in 40 ml of ethanolamine (EA) with magnetic stirring to form a homogeneous solution. The solution was transferred into a Teflon-lined stainless autoclave (50 ml capacity). The autoclave was sealed and maintained at 200 °C for 4 h and finally cooled to room temperature. White precipitate deposited on the bottom was collected by centrifugation (3,000 rpm, 5 min), washed alternately with distilled water and ethanol for several times, and dried in air at 80 °C for 4 h. Following a similar procedure, a series of ZnO samples were prepared in the different synthesis conditions by only changing one while keeping the rest to be constant.

The crystalline structure including the phase purity was examined by X-ray diffraction (XRD) via a Rigaku D/max 2500 diffractometer at the voltage of 40 kV and current of 200 mA with Cu Kα radiation ($\lambda = 0.154056$ nm), in a 2θ angular range of 20°–80° with a velocity of 6° in 1 min. The morphological features of the synthesized ZnO were investigated using a field emission scanning electron microscope (FESEM: Hitachi, S4800) operating at 5 kV. The microstructure of the product was further investigated by high-resolution transmission electron microscopy (HRTEM, FEI Tecnai G2 F20). The specific surface area of product was estimated using the BET equation based on the nitrogen adsorption isotherm (77 K) using a NOVA 2200e surface area analyzer (Quantachrome instruments, USA).

2.2 Fabrication and measurement of sensors

The structure of the gas sensor belongs to indirect heating type. The preparation and testing principle of the gas sensor are similar to that depicted in our previous report [23]. The gas sensor was fabricated as follows: the as-prepared sample was mixed and ground with distilled water in an agate mortar to form a paste. Then the paste was coated on an alumina tube, on which two platinum wires had been previously installed at each end. A small Ni–Cr alloy wire was placed through the tube as a heater, which provided operating temperature.

Gas sensing properties were measured by a CGS-8 intelligent gas sensing analysis system (Beijing Elite Tech Co. Ltd., China). The method to get different concentrations of target gas was traditional by injecting the gas to text chamber with the microinjector. The sensor resistance and response values in the air or the test gas were acquired by the analysis system automatically. The sensitivity (S) to gas was defined as: $S = R_a/R_g$, where R_a and R_g were the electric resistance in air and test gas, respectively. The time taken by the sensor to achieve 90 % of the total resistance change was defined as the response time in the case of adsorption or the recovery time in the case of desorption. The resistance measurements were carried out at optimal operating temperature. The operating temperature was controlled by adjusting the heating current.

3 Results and discussion

3.1 Phase and morphology

The morphological and structural characterizations of the prepared ZnO are shown in Fig. 1. The FESEM images in Fig. 1a, b indicate that many hollow microspheres which are composed of numerous nanorods with about several tens nanometers in diameter and 2–3 μm in length are obtained and the average size of microspheres is about 7 μm. Moreover, the numerous nanorods are radially aligned with their growth axis perpendicular to the center core, which is clearly revealed in the magnified image (Fig. 1c).

The microstructure of the product is further characterized by TEM and HRTEM, as shown in Fig. 1d, e. The TEM image (Fig. 1d) of partial hollow microsphere shows the assembly form of the constituent nanorods which conforms well to the SEM results mentioned above. The

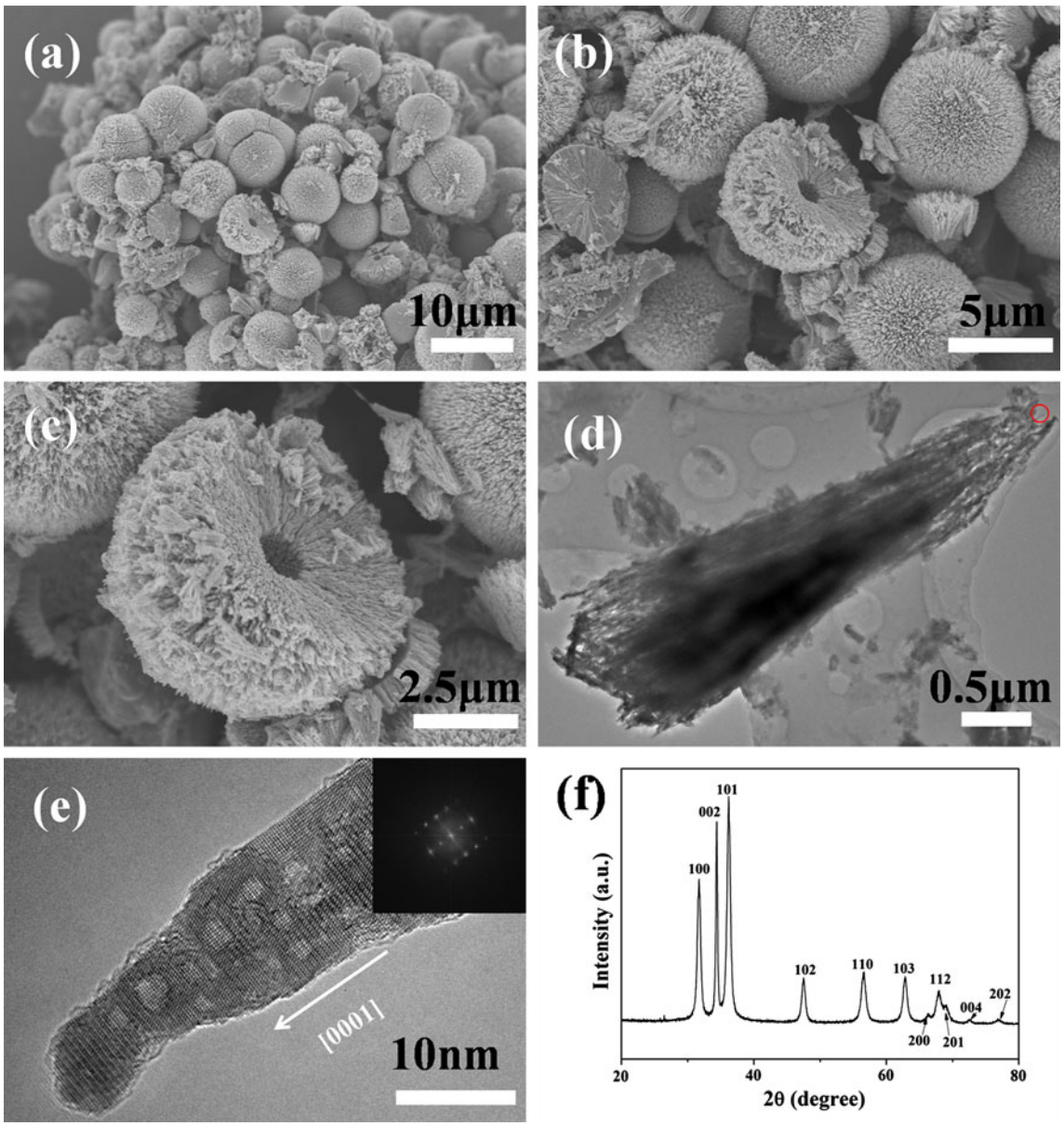

Fig. 1 The morphological and structural characterizations of the prepared ZnO: SEM images (**a**–**c**), TEM image (**d**), HRTEM image (**e**) (*inset*, corresponding two dimensional Fourier transform pattern) and XRD pattern (**f**)

HRTEM image (Fig. 1e) and the corresponding two dimensional Fourier transform pattern (Fig. 1e, inset) reveal a single-crystal entity and the preferential [0001] growth direction, which can be demonstrated by a lattice spacing of about 0.26 nm corresponding to the (002) lattice planes of ZnO. Furthermore, we can see abundant mesoporous about 2 nm are formed in the constituent nanorod, which may be due to the velocity of self-aggregation of nanograins. This phenomenon is analogous to the one reported by Yao's [14] group, where the quasi-micropores in the spindlelike nanosheets were formed by aggregation of CuO nanograins aligning along a preferential direction [010].

The corresponding XRD pattern (Fig. 1f) confirms the pure ZnO with hexagonal structure. All of the diffraction peaks can be readily indexed as hexagonal ZnO (space group: P63/mc(186)) with the lattice constants a = 3.25 Å, c = 5.207 Å, compatible with the literature values of JCPDS card no. 36-1451.

The BET measurement in Fig. 2 reveals clearly the porous character of hierarchically structured ZnO hollow spheres. The nitrogen adsorption/desorption isotherms are ascribed to type IV with large hysteresis loops, and the corresponding Barrett–Joyner–Halenda (BJH) pore size distribution plot (inset) suggests the presence of mesopores (2–50 nm) in the ZnO architectures. The BET surface area

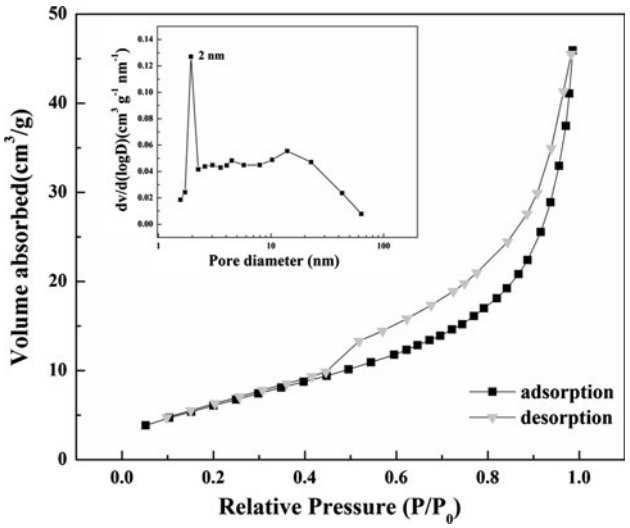

Fig. 2 Nitrogen adsorption/desorption isotherms of the ZnO hollow spheres. The *inset* is pore size distribution

is found to be 24.3 m^2/g, which is not very high because the pores embedded in the nanorods have a smaller inner surface and low pore volume, just as the report shown [12]. The calculated pore size distribution using BJH method indicated that the size of mesopores is about 2 nm (inset in Fig. 2), which is consistent with the HRTEM observation (Fig. 1e).

3.2 Growth mechanism of ZnO hollow spheres

It is known that ethanolamine molecules (EA), as a chelating ligand, exhibit coordinating ability toward metal ions due to the amino group with a lone pair of electrons in nitrogen. In solvothermal system, EA served as structure-directing agent to fabricate one-dimensional structures [24]. The linear molecular structure of EA is in favour of anisotropic growth of the ZnO to form one-dimensional structure. However, there is almost no literature about the formation of hierarchically structured ZnO in the presence of EA alone.

In order to explore the growth mechanism of ZnO nanorod-based hollow spheres, we investigated the morphology evolution of ZnO nanostructures with different reaction time and kept all other conditions constant. TEM and FESEM images of ZnO products obtained at different growth times were given in Fig. 3.

As we known, ethanolamine acted as complexing molecules in the precursor solution partially; the Zn source was primarily in the form of $[Zn(EA)_m]^{2+}$. During the solvothermal process, $[Zn(EA)_m]^{2+}$ can be slowly transformed into ZnO nuclei. The excess EA in the solution may prevent $[Zn(EA)_m]^{2+}$ from decomposing, which finally led to a lower nucleation density and rate of ZnO nuclei in the growing region. Therefore, it was found that few ZnO nuclei about 1–3 nm were formed at the reaction time of 3 h and 20 min (Fig. 3a).

EA may adsorb onto the (010) and (100) planes of the initial nuclei, which made (001) a high energy face as compared to the EA-covered (010) and (100) planes. Then subsequent growth species would prefer to attach on (001) plane of nuclei, which led to 1D growth of the ZnO finally [25]. Also, many structural defects such as pores (Fig. 1e) in some regions of the mother nanorods, characteristic of coarsening growth due to imperfectly oriented attachment, which led to densification of the spheres. As the reaction progresses, the ZnO nanorods would aggregate into nanostructures which was energetically favorable of the system. These nanorods of pure phase ZnO were aligned perpendicularly to the spherical surface, along main crystallographic axes of ZnO, pointing toward a common center, via an "oriented attachment" process [26–30]. With the extension of the reaction time to 3 h and 50 min (Fig. 3b), we obtained hollow spheres with diameter about 2 μm.

Subsequently, the ZnO crystallites located on the outer most surface would serve as nucleation seeds for the subsequent recrystallization process. The spheres still kept the structure but grew larger due to many ZnO crystal grains grew along the [0001] direction through embryos of the ZnO spheres served as nucleating centers. The process mentioned above was accompanied that smaller nanocluster particles transferred from in the interior of the spheres to surface of the spheres by Ostwald ripening [31]. Then, the inner small nanoparticles gradually disappeared, and the spheres eventually fractured into hollow spheres. As a result, spheres became hollow, more compact and larger (Fig. 3c), when the reaction time was extended to 4 h, whose average diameter was about 8 μm. After 6 h solvothermal reaction, ZnO hollow spheres became larger (about 12 μm) whereas the diameter of hollow interior became bigger and the nanorods fused into each other (Fig. 3d, e). The diameter and structural characterizations of the microspheres (Fig. 3f) did not change when the reaction time reached to 8 h.

On the above results, the solvent EA plays the critical role in the formation of the hierarchically structured ZnO. To confirm the role of EA for the formation of the ZnO microspheres, we changed the composition of solvent, while the other conditions kept unchanged. Figure 4a, b shows the SEM images of the products prepared by the solvothermal process with the EA/PEG and EA/H_2O volume ratio of 9:1 at 200 °C for 8 h. The microspheres with smaller diameter were obtained and the constituent nanorods became bigger and coarser when PEG was introduced into the system. We achieved parachute-like products when certain volume of H_2O served as solvent, which were composed of rods with diameter of several diameter aligning perpendicularly to the surface. However, when the EA/H_2O volume ratio reached to 1:1, only the pencil-like ZnO with diameter about 3 μm and the length of several tens micrometers was obtained as shown in Fig. 4c. The

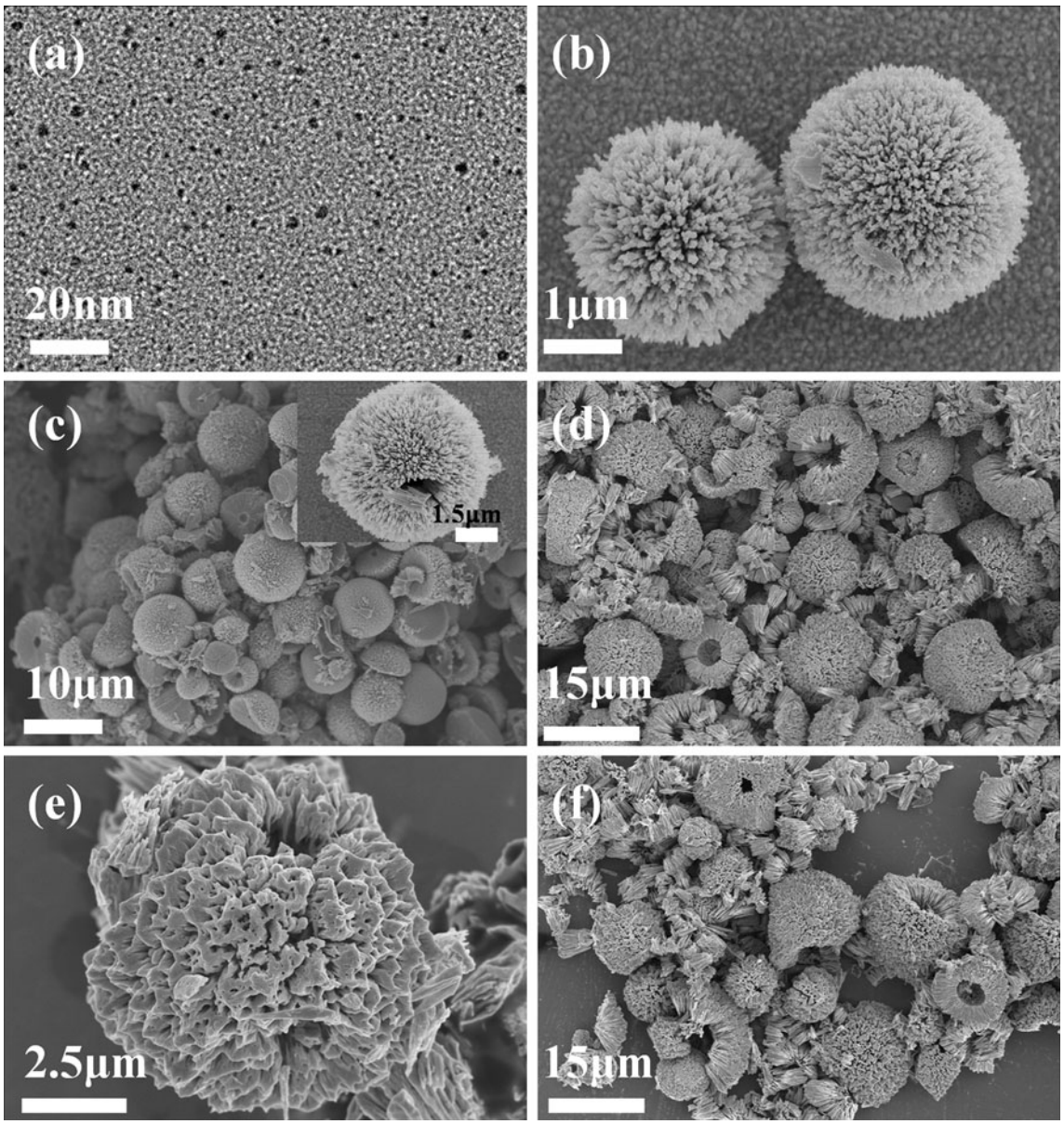

Fig. 3 TEM images of ZnO prepared at 200 °C for **a** 3 h and 20 min, FESEM images **b** 3 h and 50 min, **c** 4 h, the *inset* of **c** is the enlarged image of **c**; **d**, **e** for 6 h, and **f** for 8 h, respectively

above results confirm that the hierarchically structured ZnO microspheres were obtained when EA served as solvent alone. ZnO nuclei would grow along the preferential axis to form rods which could not assemble into microsphere when the volume ratio of water became bigger. The introduction of PEG may destroy the system of formation of hollow spheres, which need to further research.

3.3 Gas sensing properties

It is well known that temperature will affect the sensitivity of a metal oxides sensor, which can be attributed to the adsorption–desorption mechanism. In order to determine an optimal operating temperature, the responses of hollow spheres sensor to 100 ppm ethanol are measured as shown in Fig. 5. It can be seen that the response increases and reaches its maximum at 230 °C, and then decreased rapidly with the increasing temperature. At the optimum operating temperature of 230 °C, the hollow spheres show the maximum response of about 46.3. Therefore, 230 °C is chosen to be an operating temperature for further examine the properties of the hollow spheres gas sensor.

In order to investigate the gas sensing property, the gas sensors were fabricated from the as-prepared ZnO hollow spheres prepared at 200 °C for 4 h, nanorods ZnO prepared according to the report [32] and commercial particles ZnO.

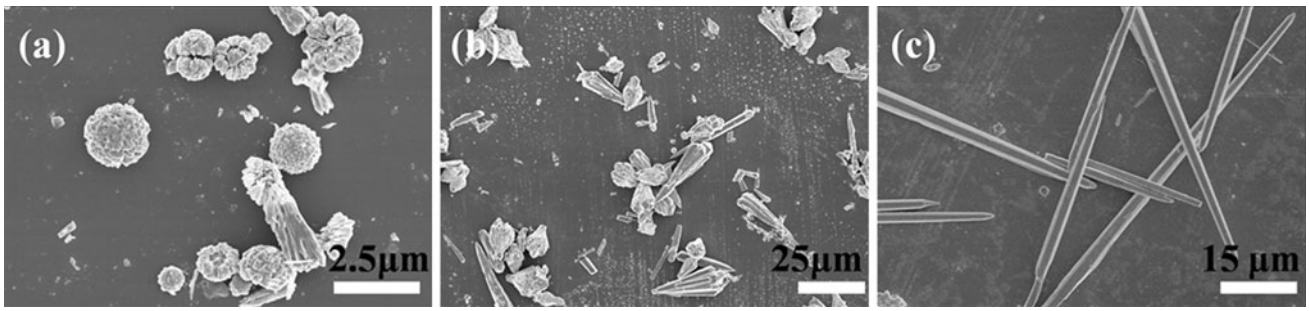

Fig. 4 FESEM images of the as-prepared ZnO samples synthesized under the volume ratio of EA/PEG 9:1 (**a**), EA/H_2O 9:1 (**b**), EA/H_2O 1:1 (**c**) at 200 °C for 8 h

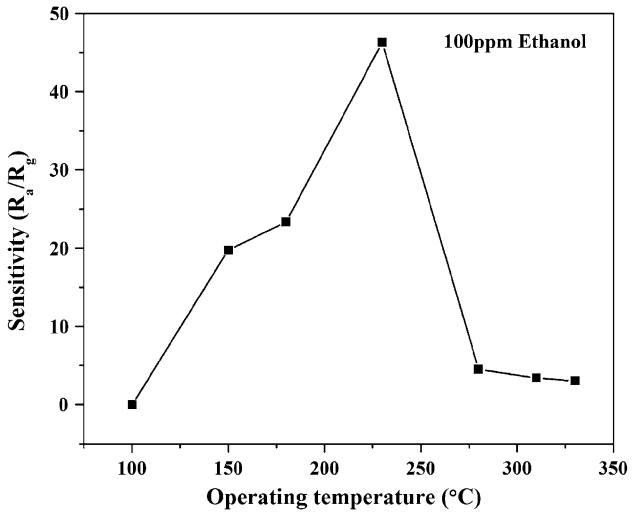

Fig. 5 Sensor response toward 100 ppm of ethanol as a function of operating temperature

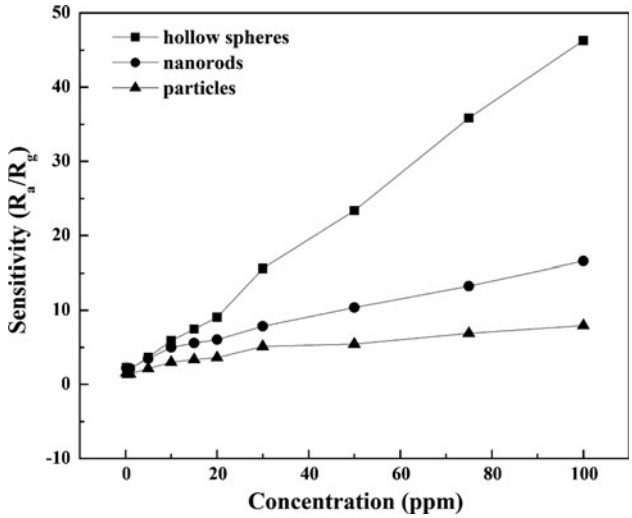

Fig. 6 Gas response to 0.25–100 ppm ethanol of the ZnO hollow spheres, nanorods, commercial powder ZnO at 230 °C

The responses of gas sensors based on ZnO with different morphologies to different ethanol concentrations at 230 °C are shown in Fig. 6. It shows clearly that the response amplitudes of the three sensors are increased on increasing gas concentration. The sensing characteristics are found to be highly dependent upon the morphology of ZnO. It can be seen that the sensors based on ZnO hollow spheres and nanorods have similar sensitivities in the low concentration range (from 0.25 to 10 ppm). With the increase of ethanol concentration, the hollow spheres sensor possesses much higher sensitivities. For 100 ppm ethanol, the sensitivity (46.3) of the ZnO hollow spheres sensor is nearly three times higher than that (16.6) of the nanorods sensor. However, the sensor sensitivity of the commercial powder is the minimum, which is only 7.9 for 100 ppm ethanol. The significant distinction of sensitivity among the three sensors is consistent with previous studies [33, 34] which have proven that hierarchical structures could significantly enhance the sensor performance.

As we all know, gas-sensing mechanism of ZnO-based sensors belongs to surface-controlled type, that is, the resistance change is controlled by the species and amount of chemisorbed oxygen on surface. Experimentally in this work, structural characteristics and large surface area could be used to explain the excellent sensitivity of the ZnO hollow spheres sensor. Firstly, there are many structural defects such as pores in the constituent nanorods according to the TEM result (Fig. 1e), which is beneficial to improve the formation of oxygen species and provide many channels to transportation of target gases. Secondly, the hierarchical structures can usually provide a large surface-to-volume ratio, which is most favorable for the diffusion of target gases in sensor materials. The BET surface area of the ZnO hollow spheres is found to be 24.3 m^2/g and the nanorods is 6.4 m^2/g, while the commercial powder is 4.5 m^2/g. In conclusion, the as-prepared ZnO hollow spheres exhibit the best gas sensing properties.

Figure 7a shows the dynamic response and recovery curve of the ZnO hollow spheres as the ethanol gas sensor, and the operating temperature is 230 °C. It is clearly shown that the sensor response is enhanced with the increase of ethanol concentration. When exposed to 0.25 ppm ethanol,

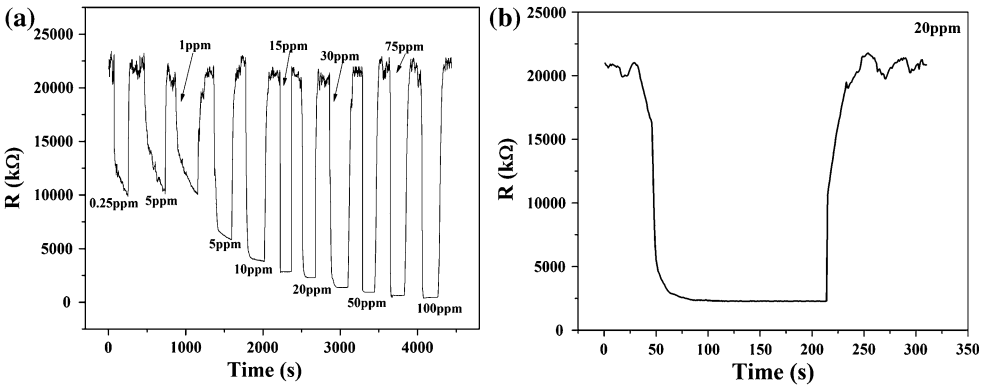

Fig. 7 **a** Dynamic response–recovery curve of the sensor based on the prepared ZnO hollow spheres to ethanol with concentrations ranging from 0.25 ppm to 100 ppm at 230 °C. **b** Transient response of the sensor to 20 ppm ethanol at 230 °C

the sensor sensitivity is about 2.3, which indicates that the sensor has the capacity to detect ethanol even at lower concentrations down to sub-ppm level. With increasing ethanol concentration, the sensitivity increases significantly. For 100 ppm ethanol, the sensitivity reaches to 46.3 which is higher than those for ZnO nanorod arrays (17) [35], porous flower-like ZnO nanosheets (21.8) [36] and porous ZnO spheres (25) [37]. Furthermore, Fig. 7b shows the response and recovery time of the ZnO hollow spheres are about 24 s and 38 s, when the concentration of ethanol is 20 ppm, indicating the high response speed for the sensor.

The selectivity of ZnO hollow spheres sensor was investigated by comparing the gas responses to ethanol, ammonia (NH_3), methanol (CH_3–OH), toluene (C_6H_5–CH_3) and xylene (CH_3–C_6H_4–CH_3) with the same concentration, which is shown in Fig. 8. The gas response toward 100 ppm ethanol is 46.3, whereas the sensitivities to 100 ppm NH_3, CH_3–OH, C_6H_5–CH_3 and CH_3–C_6H_4–CH_3 are much lower at 230 °C, especially the response to 100 ppm NH_3 is only 3.76. These results demonstrate the prepared ZnO shows higher selectivity to ethanol than to other gases.

Previous studies have shown that oxygen molecules would adsorb on the surface when the semiconductor materials are exposed to air, the oxygen molecules would be formed as negative oxygen ions, such as O^{2-}, O_2^-, and O^-, which would desorb from the surface at 80, 130 and 500 °C, respectively. Therefore, in the temperature range used, only O^- species which are stable ones, will react with ethanol [38]. This can be explained by the following reactions.

$$O_2\,(\text{gas}) \rightarrow O_2\,(\text{adsorbed}) \quad (1)$$

$$O_2\,(\text{absorbed}) + e^- \rightarrow O_2^- \quad (2)$$

$$O_2^- + e^- \rightarrow 2O^- \quad (3)$$

The electrons transfer from the conduction band to the chemisorbed oxygen result in the decrease in the electron concentration in the nanostructures. As a consequence, an increase in the resistance of the nanostructures is observed. As we know, ethanol gas would undergo two routes of decomposition reactions, dehydration and dehydrogenation

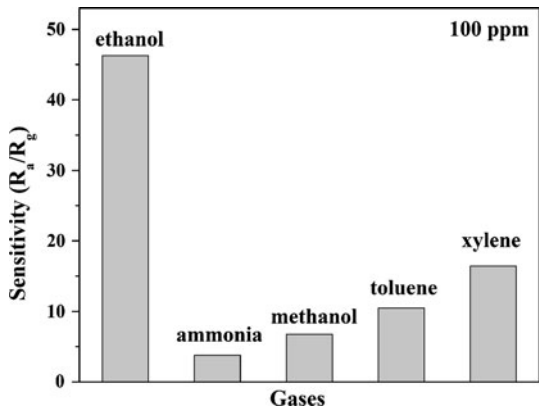

Fig. 8 Response values of the ZnO hollow spheres to different gases of 100 ppm

at operating temperature, depending on the acid–base properties of oxide catalysts used [39]. The following two reactions would explain this.

$$C_2H_5OH \rightarrow C_2H_4 + H_2O\ (\text{acidic oxide}) \quad (4)$$

$$C_2H_5OH \rightarrow CH_3CHO + H_2\ (\text{basic oxide}) \quad (5)$$

ZnO is a basic oxide, so dehydrogenation is favored. The CH_3CHO intermediate is subsequently oxidized to form CO_2 and H_2O, as depicted in following

$$CH_3CHO\,(\text{ad}) + 5O^- \rightarrow 2CO_2 + 2H_2O + 5e^- \quad (6)$$

The above reactions indicate that the electron-donating effect of ethanol gas is stronger than that of other gases. This phenomenon could explain why the response to ethanol is higher than other gases at the same concentration.

4 Conclusions

In summary, we have developed a simple and one-step solvothermal method to synthesize the hierarchically structured ZnO hollow spheres consisting of ZnO nanorods with diameter of several tens nanometers and length of 2–3 μm using ethanolamine as solvent without other

additive. By investigating the morphology evolution of ZnO nanostructures with different reaction time and changing the composition of solvent, a possible formation mechanism is proposed, from which we find the ethanolamine solvent play the critical role in the formation of the ZnO hollow spheres. The results also indicate that the sensor based on the prepared ZnO hollow spheres exhibit good ethanol sensing performance, which can be attributed to its structural defects and high surface-to-volume ratio that significantly facilitates the absorption of oxygen species and diffusion of target gas. Besides, this type of sensor shows high selectivity to ethanol, which could be a good candidate for ethanol detection.

Acknowledgments The authors are grateful for financial support from the National Natural Science Foundation of China (Grant No. 51172157).

References

1. M.H. Huang, S. Mao, H. Feick, H.Q. Yan, Y.Y. Wu, H. Kind, E. Weber, R. Russo, P.D. Yang, Science **292**, 1897 (2001)
2. T. Ganesha, S.S. Bhande, R.S. Manea, S.H. Han, Scr. Mater. **69**, 291–294 (2013)
3. W.W. Guo, T.M. Liu, Z.P. Gou, W. Zeng, Y. Chen, Z.C. Wang, J. Mater. Sci.: Mater. Electron. **24**, 1764–1769 (2013)
4. Q.D. Zhao, M. Yu, T.F. Xie, L.L. Peng, P. Wang, D.J. Wang, Nanotechnology **19**, 245706 (2008)
5. S.L. Patil, S.G. Pawar, A.T. Mane, M.A. Chougule, V.B. Patil, J. Mater. Sci.: Mater. Electron. **21**, 1332–1336 (2010)
6. S.S. Nath, M. Choudhury, D. Chakdar, G. Gope, R.K. Nath, Sens. Actuators, B **148**, 353–357 (2010)
7. X.L. Li, F.Q. Zhang, C. Ma, S. Elingarami, N.Y. He, J. Nanosci. Nanotechnol. **13**, 5859–5863 (2013)
8. O. Lupana, G.Y. Chai, C. Lee, Microelectron. J. **38**, 1211–1216 (2007)
9. L. Nasi, D. Calestani, F. Fabbri, P. Ferro, T. Besagni, P. Fedeli, F. Licci, R. Mosca, Nanoscale **5**, 1060–1066 (2013)
10. T. Hu, B.D. Liu, F. Yuan, Z.E. Wang, N. Huang, G.F. Zhang, B. Dierre, N. Hirosaki, T. Sekiguchi, J. Nanosci. Nanotechnol. **13**, 5744–5749 (2013)
11. J. Zhang, S.R. Wang, Y. Wang, M.J. Xu, H.J. Xia, S.M. Zhang, W.P. Huang, X.Z. Guo, S.H. Wu, Sens. Actuators B **139**, 411–417 (2009)
12. J. Zhang, S.R. Wang, M.J. Xu, Y. Wang, B.L. Zhu, S.M. Zhang, W.P. Huang, S.H. Wu, Cryst. Growth Des. **9**, 3532–3537 (2009)
13. J.Y. Zhong, C.B. Cao, Y.Y. Liu, Y.N. Li, W.S. Khan, Chem. Commun. **46**, 3869–3871 (2010)
14. Y. Qin, F. Zhang, Y. Chen, Y.Y. Zhou, J. Li, A.W. Zhu, Y.P. Luo, Y. Tian, J.H. Yang, J. Phys. Chem. C **116**, 11994–12000 (2012)
15. X.Z. Wang, W. Liu, J.R. Liu, F.L. Wang, J. Kong, S. Qiu, C.Z. He, L.P. Luan, Appl. Mater. Int. **4**, 817–825 (2012)
16. P. Song, Q. Wang, Z.X. Yang, Mater. Lett. **86**, 168–170 (2012)
17. Y. Li, M. Zheng, L. Ma, M. Zhong, W. Shen, Inorg. Chem. **47**, 3140–3143 (2008)
18. L.L. Wang, H.Y. Wang, Y.Q. Wang, X.J. Li, Mater. Res. Bull. **47**, 2178–2181 (2012)
19. Z.H. Jing, J.H. Zhan, Adv. Mater. **20**, 4547–4551 (2008)
20. T.H. Lea, Q.D. Truong, T. Kimura, H.H. Li, C.S. Guo, S. Yin, T. Sato, Y.C. Ling, Ceram. Int. **38**, 5053–5059 (2012)
21. D.F. Zhang, L.D. Sun, J. Zhang, Z.G. Yan, C.H. Yan, Cryst. Growth Des. **8**, 3609–3615 (2008)
22. H. Zhang, J.B. Wu, C.X. Zhai, N. Du, X.Y. Ma, D. Yang, Nanotechnology **18**, 455604 (2007)
23. P. Gao, H.M. Ji, Y.G. Zhou, X.L. Li, Thin Solid Films **520**, 3100–3106 (2012)
24. S.K. Li, Z.G. Wu, W.H. Li, Y. Liu, R.F. Zhou, D. Yan, W. Jun, P.X. Yan, CrystEngComm **15**, 1571–1577 (2013)
25. N.N. Jiang, R. Wu, J. Li, Y.F. Sun, J.K. Jian, J. Alloys Compd. **536**, 85–90 (2012)
26. X.W. Lou, H.C. Zeng, J. Am. Chem. Soc. **125**, 2697–2704 (2003)
27. B. Liu, H.C. Zeng, J. Am. Chem. Soc. **125**, 4430–4431 (2003)
28. R.L. Penn, J.F. Banfield, Science **281**, 969–971 (1998)
29. B. Liu, H.C. Zeng, J. Am. Chem. Soc. **126**, 16744–16746 (2004)
30. S. Manna, K. Das, S.K. De, Appl. Mater. Int. **2**, 1536–1542 (2010)
31. M. Mo, J.C. Yu, L. Zhang, S.K.A. Li, Adv. Mater. **17**, 756–760 (2005)
32. S.L. Bai, L.Y. Chen, R.X. Luo, IEEE Sens. J. **11**, 1969–1974 (2011)
33. J.R. Huang, Y.J. Wu, C.P. Gu, M.H. Zhai, Y.F. Sun, J.H. Liu, Sens. Actuators B **155**, 126–133 (2011)
34. B.X. Li, Y.F. Wang, Superlattices Microstruct. **49**, 433–440 (2011)
35. S.S. Ma, R. Li, C.P. Lv, W. Xu, X.L. Gou, J. Hazard. Mater. **192**, 730–740 (2011)
36. C.P. Gu, J.R. Huang, Y.J. Wu, M.H. Zhai, Y.F. Sun, J.H. Liu, J. Alloys Compd. **509**, 4499–4504 (2011)
37. W.C. Wang, Y.T. Tian, X.C. Wang, H. He, Y.R. Xu, C. He, X.J. Li, J. Mater. Sci. **48**, 3232–3238 (2013)
38. P.P. Sahay, J. Mater. Sci. **40**, 4383–4385 (2005)
39. T. Jinkawa, G. Sakai, J. Tamaki, N. Miura, N. Yamazoe, J. Mol. Catal. A Chem. **155**, 193–200 (2000)